NEUROSCIENCE

Locus coeruleus norepinephrine activity mediates sensory-evoked awakenings from sleep

Hanna Hayat[1], Noa Regev[1], Noa Matosevich[2], Anna Sales[3], Elena Paredes-Rodriguez[3,4,5], Aaron J. Krom[1,6], Lottem Bergman[1], Yong Li[3], Marina Lavigne[7], Eric J. Kremer[7], Ofer Yizhar[8], Anthony E. Pickering[3,9], Yuval Nir[1,2,10]*

A defining feature of sleep is reduced responsiveness to external stimuli, but the mechanisms mediating sensory-evoked arousal remain unclear. We hypothesized that reduced locus coeruleus (LC) norepinephrine (NE) activity during sleep mediates unresponsiveness, and its action promotes sensory-evoked awakenings. We tested this using electrophysiological, behavioral, pharmacological, and optogenetic techniques alongside auditory stimulation in freely behaving rats. We found that systemic reduction in NE signaling lowered probability of sound-evoked awakenings (SEAs). The level of tonic LC activity during sleep anticipated SEAs. Optogenetic LC activation promoted arousal as evident in sleep-wake transitions, EEG desynchronization, and pupil dilation. Minimal LC excitation before sound presentation increased SEA probability. Optogenetic LC silencing using a soma-targeted anion-conducting channelrhodopsin (stGtACR2) suppressed LC spiking and constricted pupils. Brief periods of LC opto-silencing reduced the probability of SEAs. Thus, LC-NE activity determines the likelihood of sensory-evoked awakenings, and its reduction during sleep constitutes a key factor mediating behavioral unresponsiveness.

INTRODUCTION

Sleep is characterized by a reversible disconnection from the environment that entails reduced responsiveness to external stimuli. An elevated arousal threshold is a central feature of sleep that is present in all mammals and constitutes the main criterion by which sleep is defined in species lacking cortical electroencephalography (EEG) such as reptiles, nematodes, flies, and fish, and even in jellyfish without a central nervous system (1). Thus, understanding how sleep is maintained in the face of external sensory events and what determines sensory-evoked awakening is an open question. Naturally, the intensity of sensory stimuli affects awakening probability (2), but other factors such as behavioral relevance also play a role. For example, vocalizing a person's name is more likely to produce awakening compared to a meaningless stimulus of equal intensity (3). Apart from the properties of sensory stimuli, the internal state also plays a role. For example, arousal thresholds depend on sleep stage [non-rapid eye movement (NREM) sleep versus rapid eye movement (REM) sleep], sleep duration, and slow-wave activity (SWA) (2). In addition, arousal thresholds vary substantially between individuals and with age (4): While some individuals experience hyperarousal (e.g., chronically or during transient anxiety) and wake up frequently from weak stimuli, others sleep deeply and only high-intensity stimuli lead to awakenings. What determines sensory-evoked awakening and the factors underlying variability across individuals, age, and throughout sleep remain largely unknown.

Wakefulness is supported by a number of subcortical wake-promoting neuromodulatory systems (5). Multiple studies established that levels of norepinephrine (NE), serotonin, histamine, and hypocretin (orexin) are high during wakefulness and low during both NREM and REM sleep, whereas acetylcholine levels and dopaminergic levels (in the ventral tegmental area and in the ventral periaqueductal gray matter) are high during both wakefulness and REM sleep and decrease during NREM sleep (5, 6). Recent studies established a causal relationship between neuromodulatory activity and awakenings. For example, optogenetic activation of hypocretin neurons in the lateral hypothalamus (7), noradrenergic neurons in the locus coeruleus (LC) (8, 9), and dopaminergic neurons in the dorsal raphe nuclei (10) increases the probability of sleep-to-wake transitions. Activating GABAergic neurons from the lateral hypothalamus or dopaminergic neurons in the ventral tegmental area induces rapid awakening from NREM, but not REM sleep (11, 12). However, these experiments focused on internally triggered sleep-to-wake transitions, and it remains unclear whether the same systems also mediate sensory-evoked awakenings.

We hypothesized that the LC-NE system plays a key role in mediating sensory-evoked arousals and that its reduced activity throughout sleep contributes to unresponsiveness. Several lines of evidence support this proposition: First, LC activity was found to be high during wakefulness, low during NREM sleep, silent during REM sleep, and to increase before sleep-to-wake transitions in rats (13). Second, LC activation leads to EEG activation in anesthetized rats (14) and immediate awakening from sleep (8, 9)—within few seconds—whereas activation of hypocretin neurons leads to an awakening with latencies around 25 s (7), and those are likely mediated via LC projections (15). Third, LC-NE activity is implicated in orienting responses and in responding to salient behaviorally relevant stimuli (16) and is involved in stress and pain processing that affects arousals and awakenings (17, 18). Fourth, LC-NE modulates

[1]Department Physiology and Pharmacology, Sackler School of Medicine, Tel Aviv University, Tel Aviv, Israel. [2]Sagol School of Neuroscience, Tel Aviv University, Tel Aviv, Israel. [3]School of Physiology, Pharmacology and Neuroscience, University of Bristol, Bristol BS8 1TD, UK. [4]Department of Pharmacology, Faculty of Medicine and Nursing, University of the Basque Country (UPV/EHU), 48940 Leioa, Spain. [5]Neurodegenerative Diseases Group, Biocruces-Bizkaia Health Research Institute, 48903 Barakaldo, Spain. [6]Department of Anesthesiology and Critical Care Medicine, Hadassah-Hebrew University Medical Center, Hebrew University–Hadassah School of Medicine, Jerusalem, Israel. [7]Institute de Génétique Moléculaire de Montpellier, University of Montpellier, CNRS, Montpellier, France. [8]Department of Neurobiology, Weizmann Institute of Science, Rehovot, Israel. [9]Department of Anaesthesia, University Hospitals Bristol, Bristol BS2 8HW, UK. [10]Functional Neurophysiology and Sleep Research Laboratory, Tel-Aviv Sourasky Medical Center, Tel Aviv 64239, Israel.
*Corresponding author. Email: yuvalnir.tau@gmail.com
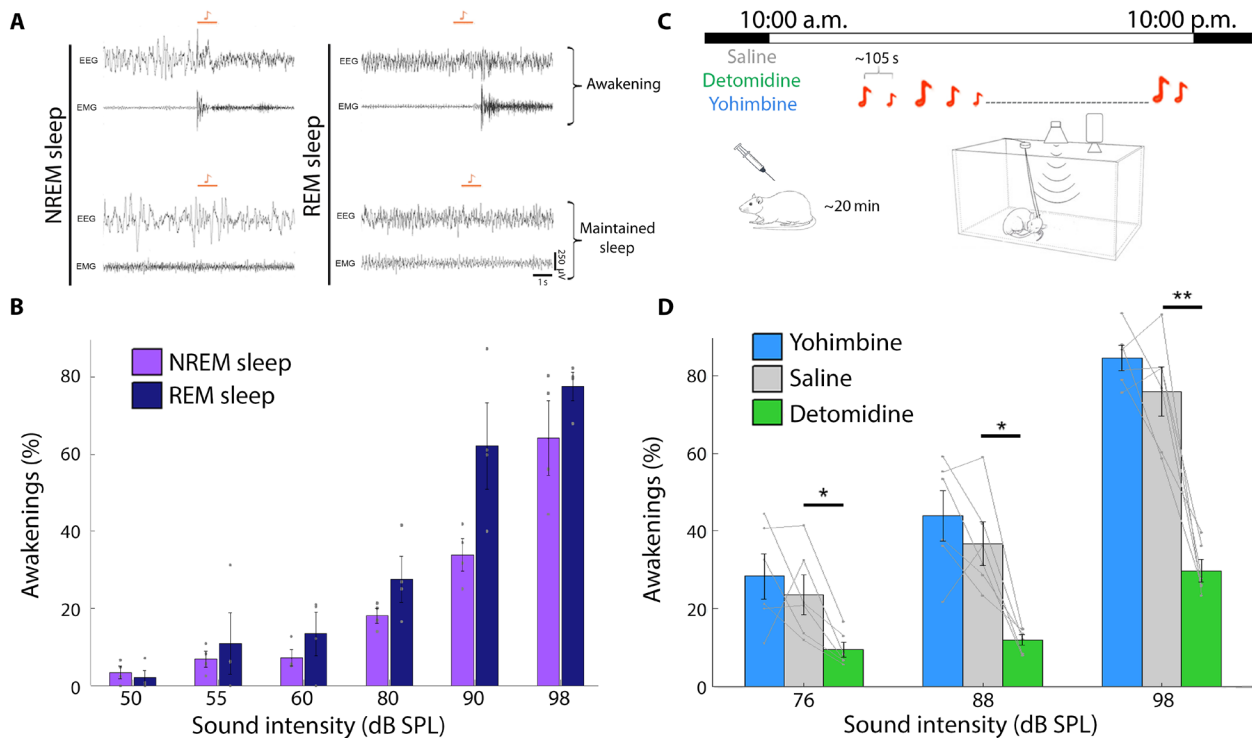
Fig. 1. Lower NE signaling decreases the probability of SEAs from NREM sleep. (**A**) Representative EEG and EMG traces showing immediate awakenings (top) versus maintained sleep (bottom) after auditory stimulation (4-kHz pure tone, 1-s duration; orange bars) in NREM sleep (left) and REM sleep (right). (**B**) Probability of awakenings (%) as a function of sound intensity in NREM sleep (purple) and REM sleep (dark blue). Gray circles show individual subject data ($n = 4$ rats). (**C**) Schematic of experimental setup for rat arousal threshold experiments (each lasting ~12 hours during lights on periods, with ~400 tone pips presented every 105 s on average). Sounds were delivered intermittently from speaker on top, while animals were continuously monitored with EEG, EMG, and video. In pharmacological experiments, NE drugs were injected intraperitoneally at lights on (10:00 a.m.). (**D**) Probability of awakenings (%) as a function of sound intensity in NREM sleep following administration of detomidine (α2 agonist, lower NE; green), yohimbine (α2 antagonist, higher NE; blue), or saline (gray). Note that lower NE decreases awakening probability. Two-way repeated-measures (RM) ANOVA, followed by post hoc t tests corrected with false discovery rate (FDR) *$P < 0.05$ and **$P < 0.01$ in $n = 6$ rats.

the signal-to-noise ratio in sensory systems (*19*). Fifth, a higher arousal threshold is found in NE-deficient mice after sleep deprivation (*20*), and low NE levels during wakefulness are associated with electrophysiological markers of disengagement from the environment such as high-voltage spindles (*21*). Given these considerations, we set out to test the causal role of LC-NE activity in mediating sensory disconnection during sleep.

We performed a series of experiments in rats, focusing on auditory stimulation during natural sleep where we controlled sensory stimulation with high temporal resolution. After establishing an experimental system to quantify auditory arousal thresholds from natural sleep, we pharmacologically manipulated NE signaling, finding that lower NE signaling reduced awakening probability. Next, we recorded LC spiking activity during natural sleep and found that baseline tonic LC activity was higher before sounds that produced awakenings. To test the causal role of LC-NE activity in more detail, we established selective and efficient optogenetic control over LC activity, including the use of a new vector to silence the LC. Both optogenetic excitation and silencing reliably controlled LC activity and bidirectionally modulated pupil size. We then delivered sounds during natural sleep in conjunction with either minimal LC excitation or with LC silencing, finding that LC-NE activity is sufficient (and necessary) to modulate the probability of awakening in response to sound.

RESULTS

Attenuation of NE signaling decreases the probability of sound-evoked awakening

We first established and validated an experimental protocol to reliably quantify auditory arousal threshold in freely sleeping rats. We continuously monitored the vigilance state via EEG, electromyography (EMG), and video as animals spontaneously switched between wakefulness and sleep. In each experiment lasting 10 to 12 hours, hundreds of tone pips were intermittently presented with long interstimulus intervals, and for each trial, we determined whether the stimulus led to an awakening or sleep was maintained (Fig. 1A, fig. S3, and Materials and Methods). The probability of sound-evoked awakening (SEA) monotonically increased with sound intensity levels and also depended on sleep stages whereby REM sleep was associated with higher SEA probability (Fig. 1B). Two-way analysis of variance (ANOVA) revealed significant main effects of both sound intensity ($P = 3.29 \times 10^{-15}$) and sleep stage ($P = 0.028$, $n = 4$ rats). The increase in awakening probability as a function of sound intensity established that arousal threshold can be quantified in a sensitive and reliable manner using this approach. In addition, we find higher EEG SWA (0.5 to 4 Hz power) in prestimulus baseline (2 s before sound onset) before trials not followed by behavioral awakenings (fig. S3G), as previously shown (*2*).

We then evaluated SEA probability after manipulating NE signaling with drugs affecting the α2 adrenoceptor [whose primary effect
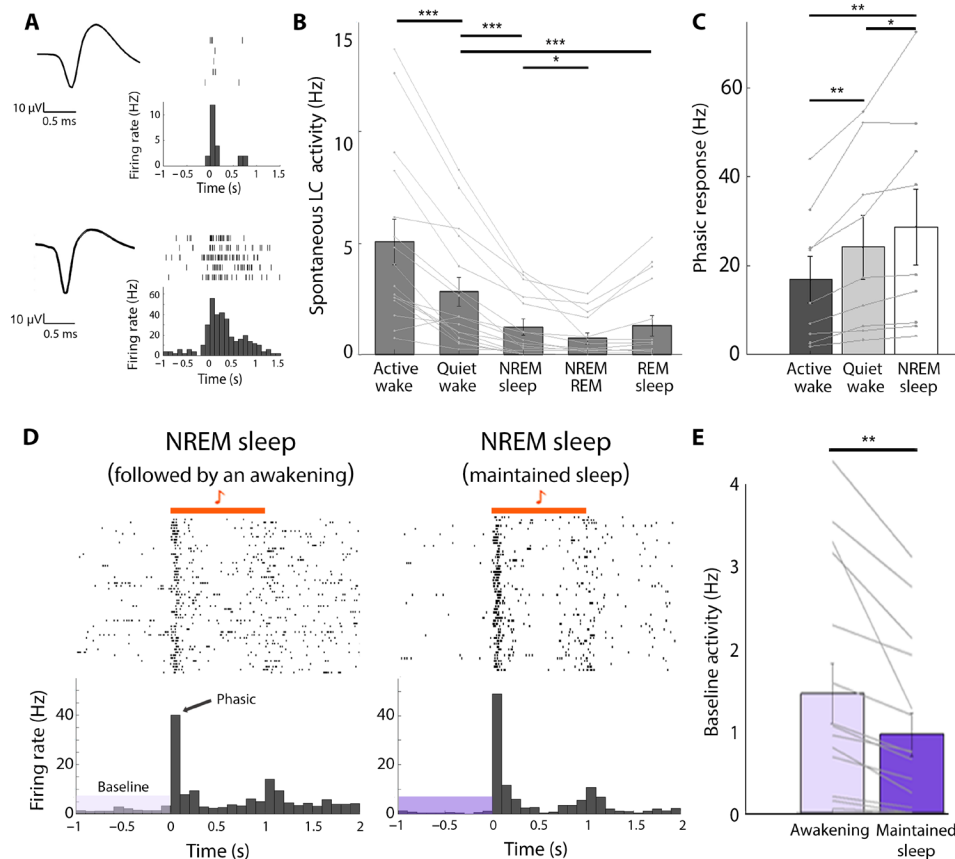
Fig. 2. Baseline tonic LC activity is higher before SEAs from NREM sleep. (A) Two representative LC clusters recorded during the experiment. Left: Action potential waveforms of unit clusters. Right: Corresponding raster plot and peristimulus time histogram (PSTH) in response to toe pinch under light anesthesia. **(B)** Average spontaneous firing rates of LC clusters ($n = 16$ from three rats) across different sleep-wake states, one-way RM ANOVA followed by post hoc FDR-corrected t test (***$P < 0.001$ and *$P < 0.05$). **(C)** Phasic LC response to sound (0 to 100 ms after sound onset) in 9 of 16 LC neurons exhibiting auditory-evoked discharges as a function of vigilance state. Mean ± SEM across $n = 9$ clusters, one-way RM ANOVA followed by post hoc FDR-corrected t-test; *$P < 0.05$ and **$P < 0.01$. **(D)** Representative auditory-evoked multiunit (MU) firing (raster and PSTH) during NREM sleep. Left: Trials followed by awakening. Right: Trials followed by maintained sleep. Horizontal orange bar shows 1-s tone stimulus. **(E)** Quantification of baseline LC activity during NREM sleep in trials preceding awakening (light purple) versus maintained sleep (dark purple). Data represent means ± SEM (**$P < 0.01$, paired t test; $n = 16$ neuronal clusters, an average of 84 trials per cluster, $n = 3$ rats). Note significantly higher baseline activity before awakenings (51.37% increase compared with maintained sleep).

is suppression of NE release via autoreceptor negative feedback; (*22*)]. We injected either detomidine (α2 agonist, to decrease NE signaling; 1 mg/kg), yohimbine (α2 antagonist, to increase NE signaling; 1 mg/kg), or saline (control) intraperitoneally to each animal in separate experiments performed on different days with order counterbalanced (Fig. 1C). We first evaluated the effects of modulating NE signaling on sleep architecture and locomotor activity (fig. S1). Detomidine increased the time spent in NREM sleep at the expense of wakefulness and REM sleep (20.2 ± 1.1% increase in NREM sleep, $n = 6$ rats; fig. S1B). Yohimbine did not significantly affect sleep architecture but did increase locomotor activity during the first 3 hours (fig. S1, D and E). Next, we evaluated SEAs after NE drug injections. Detomidine decreased the probability of SEA during NREM sleep [14.1 ± 3.4%, 24.8 ± 5.0%, and 46.1 ± 7.3% decrease for 76-, 88-, and 98-dB SPL (sound pressure level) sound levels, respectively; $n = 6$ rats] (Fig. 1D and fig. S1A). Yohimbine did not affect the probability of SEA. Although this systemic pharmacological manipulation has some caveats given the widespread actions of α2 adrenoceptor agonists, this supported the suggestion that attenuating NE signaling decreases the probability of SEA.

Baseline tonic LC activity reflects probability of SEA from NREM sleep

To determine whether ongoing changes in LC activity predict SEAs during sleep, we recorded the spiking of LC neurons ($n = 16$ neuronal clusters from three rats) using chronically implanted, drivable silicon probes in freely behaving animals. LC neurons were identified by their typical action potential waveforms and their "biphasic" responses to toe pinch (Fig. 2A). We found that mean spike discharge rates were highest during active wakefulness, lower during quiet wakefulness, and lowest in sleep (Fig. 2B), as previously reported (*13*). We did not observe differences in LC firing rates between NREM sleep and REM sleep, possibly due to our multiunit recordings. The lowest firing rates were observed during NREM-to-REM transitions, when sleep spindle activity is maximal (*23*, *24*). Many (56%, 9 of 16) LC clusters reliably responded to auditory stimulation by firing brief phasic bursts shortly after sound onset, which showed an opposite trend relative to tonic baseline firing (phasic response: active wake < quiet wake < NREM sleep, $n = 9$ clusters; Fig. 2C). Dividing auditory trials during NREM sleep to those that ultimately led to an awakening or not (Fig. 2, D and E), we found that LC spiking

activity before sound onset was significantly higher ($P < 0.01$ via paired t test) before trials that led to awakening (1.4 ± 0.4 Hz) versus maintained sleep (0.95 ± 0.3 Hz). By contrast, the phasic response (0 to 100 ms after sound onset) was not linked with SEA probability during NREM sleep ($P = 0.96$, paired t test; $n = 9$).

Optogenetic LC excitation elicits behavioral, electrophysiological, and pupillary signs of arousal

To achieve cell type–specific optogenetic control over LC activity, we unilaterally transduced LC neurons by injecting CAV2-PRS-ChR2-mCherry (Fig. 3A). Transgene expression was specific and effective, where 100% of the mCherry-positive neurons coexpressed tyrosine hydroxylase (TH) and $83 \pm 3.4\%$ of TH$^+$ neurons coexpressed mCherry (Fig. 3B). Next, we verified optical activation of LC neurons in vivo under light anesthesia. We implanted a 16-channel optrode and recorded LC firing activity in neurons in the dorsal pons, which exhibited characteristic wide action potentials and responded to both toe pinch (Fig. 3D) and laser stimulation (Fig. 3, E to I). Upon laser illumination, we found reliable activation of LC neurons that showed a clear relationship between firing rate and illumination parameters including light intensity, pulse duration, and stimulation frequency. Although a subset of LC neurons may not respond to toe pinch (25), in our hands, neurons that responded to laser stimulation showed toe pinch–evoked firing, which had a typical biphasic response to contralateral and ipsilateral pinch (Fig. 3D) (17, 26).

In freely behaving rats, strong (10 s at 10 Hz, 90-ms pulse duration) LC activation reliably led to awakenings from NREM sleep and to EEG activation, in line with previous studies (8, 9) (Fig. 3C). The ability to elicit short arousals upon unilateral LC optogenetic activation was maintained for 6 months, attesting to sustained and stable canine adenovirus type 2 (CAV2)–mediated ChR2 expression with minimal toxicity [as previously noted; (9)], also validated by immunohistochemistry (Materials and Methods).

Next, we asked whether LC opto-activation alters pupil size. Under light anesthesia, LC opto-activation (3-s stimulation, at 10 Hz) induced a large increase in pupil size (32.38, 65.03, 93.26, 127.57, and 177.30% increase compared with baseline for 10-, 30-, 50-, 70-, and 90-ms illumination pulse durations, respectively; Fig. 3, J to L, and movie S1). Together, these data demonstrate that optogenetic LC excitation elicits reliable behavioral, electrophysiological, and pupillary markers of arousal.

Minimal optogenetic LC excitation increases probability of SEAs during NREM and REM sleep

To examine the causal effects of LC activity on arousal threshold during sleep, we combined LC optogenetic activation with auditory stimulation. Pupil dilation (under light anesthesia) and awakenings during NREM sleep from adequate opto-activation were prerequisites for inclusion of rats in the in vivo auditory arousal threshold experiments. For each animal, we first titrated laser stimulation to identify a minimal level that was insufficient on its own to elicit reliable awakenings (by shortening stimulation duration to 3 s and shortening individual pulse duration to 10 or 30 ms; see Materials and Methods). Next, during the arousal threshold experiment, tone pips were delivered at 67- and 80-dB SPL. In half of auditory trials, sounds were presented on a background of minimal laser illumination. In addition, laser was activated in the absence of sound to evaluate the effect of the laser alone. We then compared awakening probability in sound-only trials ("S"), laser-only trials ("L"),

and their co-occurrence ("SL") (Fig. 4A). LC activation increased awakening probability (29.8 $\pm$ 5.9% and 25.3 $\pm$ 8.3% increase from NREM sleep and REM sleep, $n = 8$ rats and $n = 6$ rats, respectively; Fig. 4, B and C, and fig. S2). This increase was greater than that expected, assuming independent effects of LC activation and auditory stimulation (yellow bars in Fig. 4 and fig. S2; Materials and Methods). We found a change in SEA probability for all stimulation regimes (5 Hz, 10 Hz, or "phasic mode" in Materials and Methods; fig. S2). Because sleep spindles are associated with higher arousal threshold during NREM sleep (27, 28), we analyzed their occurrence during minimal LC excitation associated with increased SEA probability. LC optogenetic activation (at 10 Hz) before sounds presented during NREM sleep decreased spindle occurrence (0.052 spindles/s versus 0.036 spindles/s for "laser off" and "laser on" trials, respectively; $n = 8$ rats, $P = 0.017$ via one-tail paired t test), in agreement with previous studies (13, 24).

Optogenetic silencing with an anion-conducting channelrhodopsin effectively suppresses LC neuronal activity and causes pupil constriction

Multiple wake-promoting systems can lead to sleep-wake transitions, and as we have seen, selective LC-NE activity is sufficient to increase probability of SEA. But, does selective silencing of this system alone during sleep decrease SEAs? In other words, is LC-NE activity necessary to modulate arousal threshold? To address this, we specifically and efficiently silenced the LC with high temporal resolution using a CAV2 vector harboring a soma-targeted anion-conducting opsin stGtACR2 (29) under the control of the PRS promoter (CAV2-PRS-stGtACR2-fRed). After bilateral LC injections, we observed specific transgene expression in the LC, where 100% of the fusionRed (fRed)–positive neurons coexpressed dopamine β-hydroxylase (DBH) and $31 \pm 9.6\%$ DBH$^+$ neurons coexpressed fRed (Fig. 5A).

To evaluate the functional effects of stGtACR2 on LC neurons in vitro, we transduced rats (p21) unilaterally with CAV2-PRS-stGtACR2-fRed and, 2 to 3 weeks later, prepared acute pontine slices for whole-cell patch-clamp recordings. Recordings from transduced LC neurons ($n = 14$) showed that opto-activation of stGtACR2 silenced spontaneous firing by activating a potent shunting conductance that reversed close to the calculated chloride reversal potential (fig. S5). This was capable of blocking action potential discharge evoked by intracellular current injection (driving firing to ~15 to 20 Hz) with rapid onset and offset (Fig. 5B).

To stringently test the effectiveness of the stGtACR2 silencing strategy in vivo, we transduced adult rats unilaterally with a relatively low titer of CAV2-PRS-stGtACR2-fRed [1.4×10^7 physical particles (pp)] and, 3 to 4 weeks later, recorded LC action potential discharge under urethane anesthesia with a 32-channel silicon probe. Laser illumination of the LC, delivered via a separate optic fiber (445 nM, 10 mW at end of fiber), strongly silenced neurons, including during trials when paw pinches or foot shocks were delivered (Fig. 5, C and D).

Such LC opto-silencing led to robust pupil constriction even during light anesthesia, when pupils are already constricted at baseline. Continuous bilateral laser stimulation decreased pupil size compared with baseline ($8.2 \pm 3.66\%$ and $14.9 \pm 6.9\%$ decrease for 3- and 10-s laser pulses, respectively; $n = 6$; Fig. 5, E and F). Pupil constriction was parametrically dependent on laser stimulus duration, whereby longer illumination (10 s versus 3 s) led to a larger effect ($P < 0.05$). The average time to nadir was 3.14 ± 0.28 s after
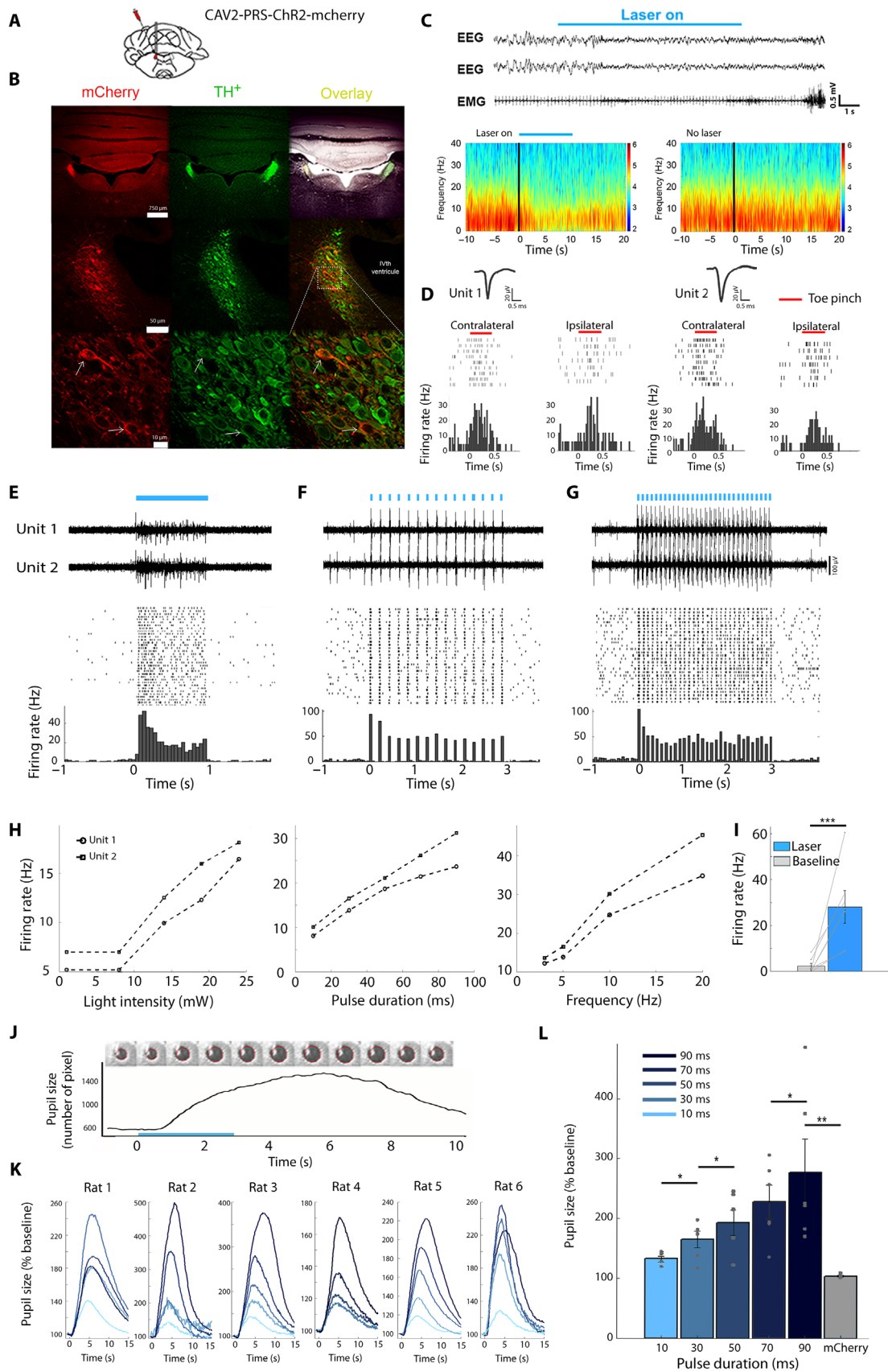
Fig. 3. Specific and effective optogenetic excitation of LC neurons. See caption on the following page.

Fig. 3. Specific and effective optogenetic excitation of LC neurons. (**A**) Schematic of unilateral LC injection and optic fiber implantation. (**B**) Specific expression of ChR2-mCherry in LC neurons: Representative coronal images showing CAV2-PRS-ChR2-mCherry expression (left column, red), labeling of TH$^+$ neurons (middle column, green), and their overlay (right column, yellow). Top: Global expression in coronal sections; middle: expression around the LC; bottom: magnified images of cells in the boxed area marked in middle row. Arrows mark neurons showing coexpression. (**C**) Top: Representative EEG and EMG traces showing an immediate awakening from NREM sleep upon strong optogenetic LC activation (10-s stimulation at 10 Hz, 90-ms pulses). Bottom: Representative EEG spectrograms after LC activation (bottom left) versus no laser stimulation (bottom right). (**D**) Representative recordings from two LC neurons recorded simultaneously. Insets show action potential waveforms, while raster plots and PSTHs show typical biphasic response to contralateral and ipsilateral toe pinch. (**E**) Top: Representative high-pass–filtered (>300 Hz) traces of two simultaneously same recorded channels in response to 1 Hz on/off laser stimulation. Middle and bottom: Raster plot and PSTH of neuron from bottom trace. (**F**) Same as in (E) for stimulation at 5 Hz (pulse duration, 10 ms). (**G**) Same as in (E) for laser stimulation at 10 Hz (pulse duration, 10 ms). (**H**) Laser-evoked firing rate as a function of light intensity (left; 1-s stimulation), pulse duration (middle; at 5 Hz), or stimulation frequency (right; pulse duration, 10 ms). (**I**) Significant increase in LC firing rates upon 1-s laser illumination compared with baseline (***$P < 0.001$, paired t test; $n = 7$ neuronal clusters from two rats, 37 trials, on average, per unit). (**J**) Representative single trial example of LC optogenetic induced pupil dilation. Top: Video images and pupil size estimation (red contour) before and during 3-s laser illumination (10 pulses/s, 90-ms pulse duration). (**K**) Fifteen-second time courses of pupil size increase (relative to baseline) for five pulse duration conditions (10 to 90 ms, light to dark blue) in each animal. (**L**) Summary data (mean ± SEM) of pupil size increase as a function of laser pulse duration (**$P < 0.01$ and *$P < 0.05$, Wilcoxon test) in $n = 6$ rats (ChR-mCherry; blue) and $n = 6$ control rats (mCherry; gray). Five to 15 trials per pulse duration condition.
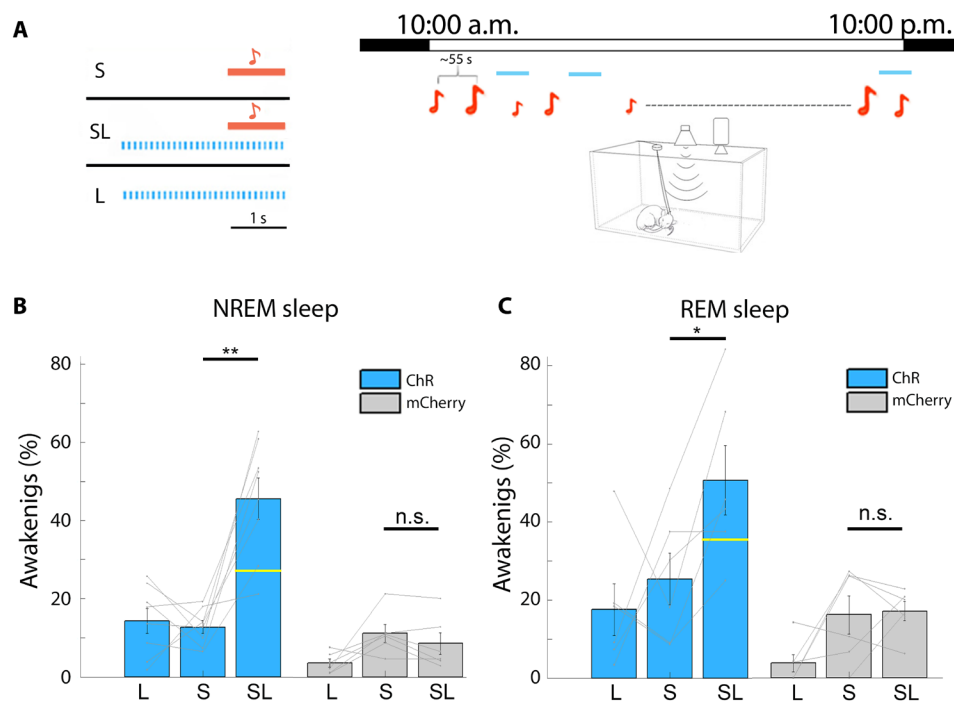

Fig. 4. Minimal optogenetic LC excitation increases the probability of SEAs. (**A**) Left: Schematic of three conditions in LC optogenetic activation arousal threshold experiments: presentation of sound (S) only, sound on a background of blue laser stimulation (SL), and blue laser only (L). Right: Schematic of experimental session for rat arousal threshold experiments combined with LC optogenetics (each experiment lasting ~12 hours during lights on periods, with hundreds of tone pips presented every 55 s on average). (**B**) Probability of awakening in NREM sleep as a function of the three experimental conditions in rats injected with CAV-PRS-ChR2-mCherry (blue, $n = 8$ rats) or control mCherry (gray, $n = 6$ rats). Yellow horizontal line dividing the SL bar represents the expected independent effect of sound and laser stimulation (Materials and Methods). n.s., not significant. (**C**) Same as in (B) for REM sleep with rats injected with CAV-PRS-ChR2-mCherry (blue, $n = 6$ rats) or control mCherry ($n = 6$ rats; gray). **$P < 0.01$ and *$P < 0.05$, paired t tests corrected with FDR (see fig. S2 for laser frequency parameters). On average, per session and for each condition (SL/S/SL), $n = 68$ trials occurred during NREM sleep, and $n = 21$ trials occurred during REM sleep.

laser onset for 3-s stimulation and 9.26 ± 0.79 s for 10-s stimulation. Thus, CAV2-mediated expression of stGtACR2 allows effective opto-silencing of LC neuronal activity, which causes pupil constriction.
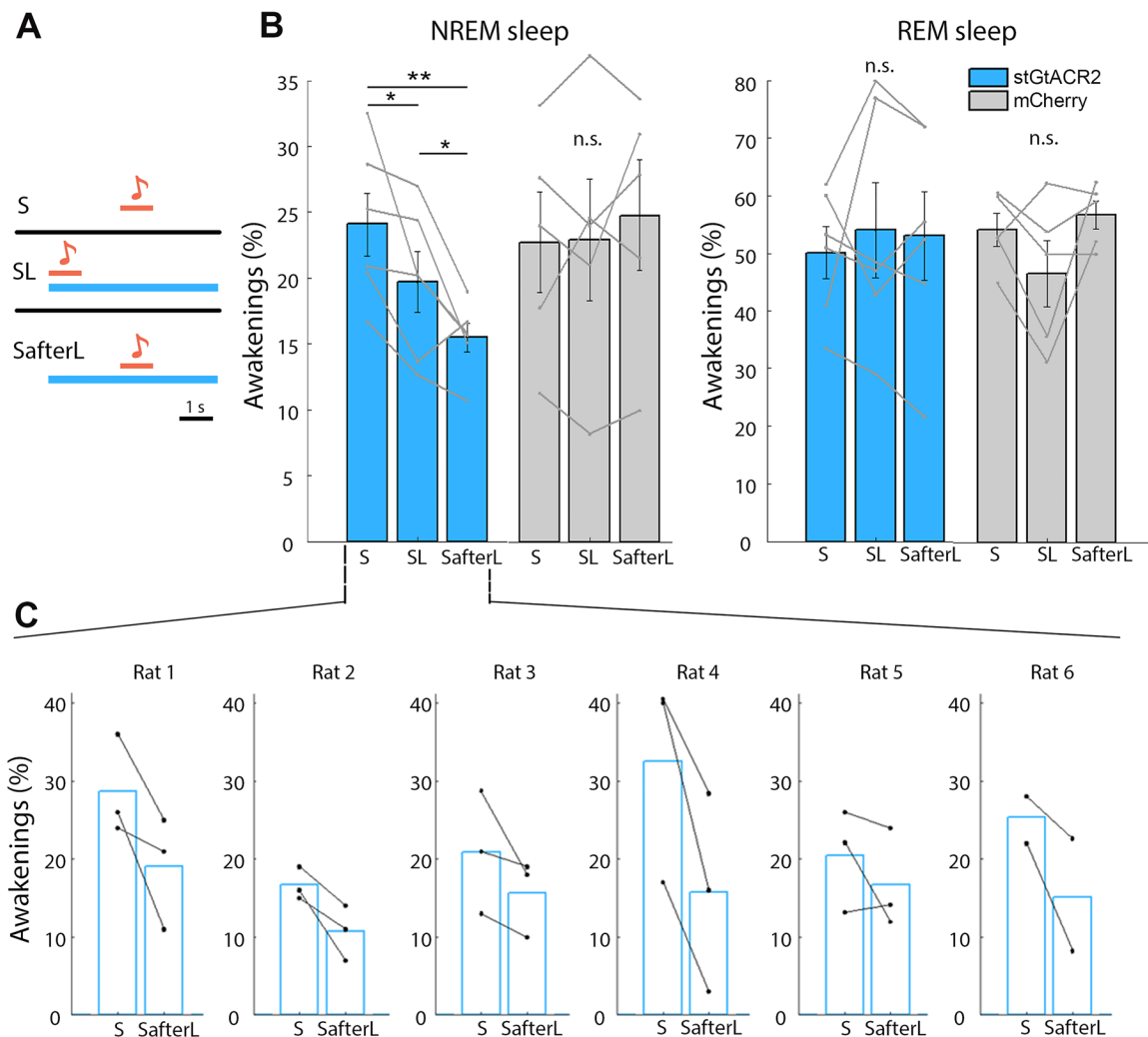
Optogenetic LC silencing decreases probability of SEA from NREM sleep

To assess whether LC silencing affects arousal thresholds during sleep, we combined LC optogenetic silencing via stGtACR2 with auditory stimulation. To ensure effective LC silencing in each

animal, pupil constriction in both eyes (under anesthesia as above) was a prerequisite for in vivo auditory arousal threshold experiments. Laser stimulation was applied for 5 s continuously to avoid effects of rebound activity upon silencing termination (5 to 7 mW at the end of the fiber), either simultaneously with the sound (SL) or—motivated by the difference in baseline tonic effects noted previously (Fig. 2)—starting 2 s before sound onset (SafterL; Fig. 6A). LC silencing increased EEG SWA in NREM sleep (fig. S3H), as was reported for LC silencing during wakefulness (8). SEA probability during NREM sleep (but not REM sleep) decreases in both conditions (4.38 ± 2.01%
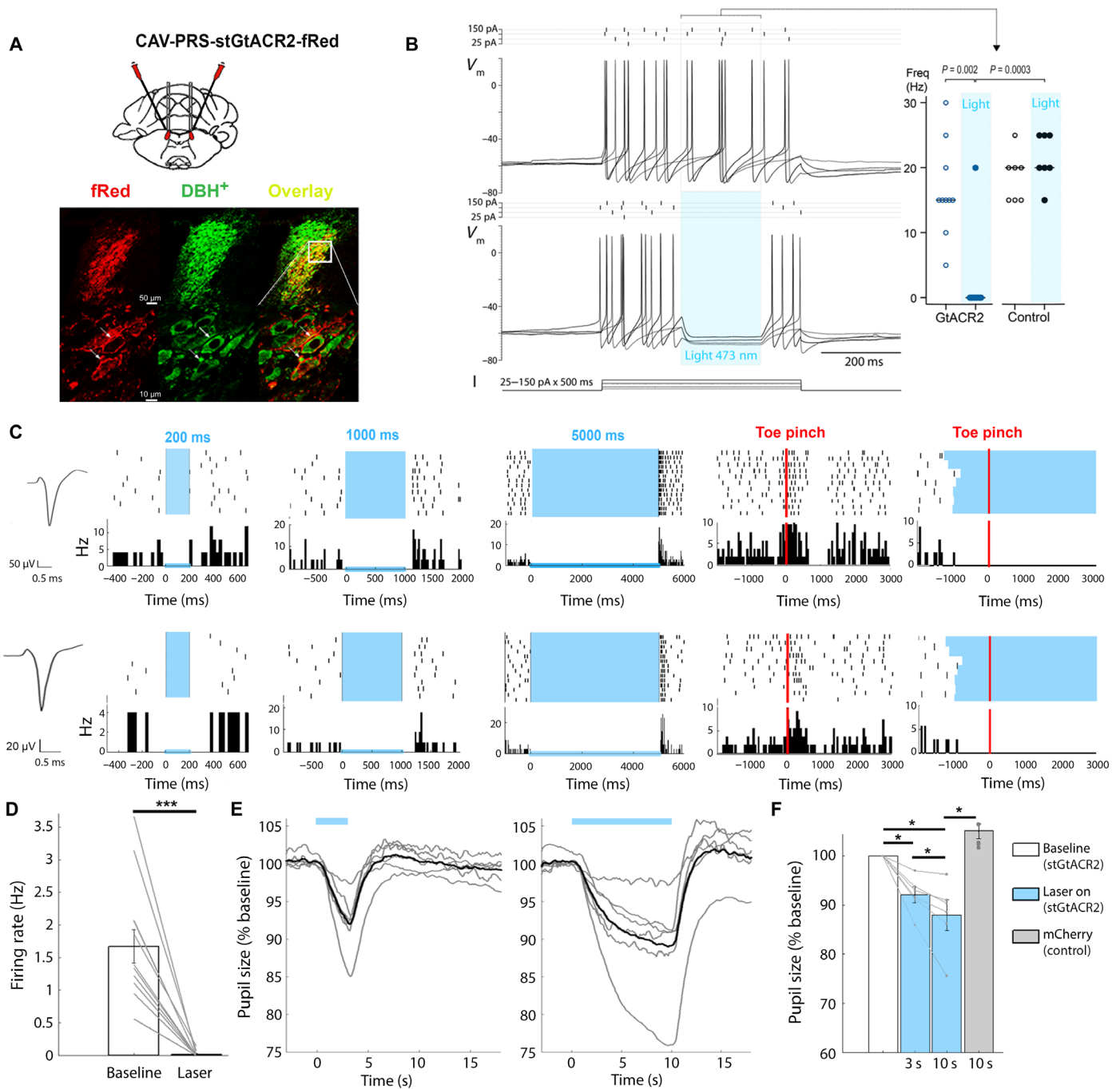
Fig. 5. Specific and effective optogenetic inhibition of LC neurons. (**A**) Schematic of bilateral LC injection and optic fiber implantation (top) and specific expression of stGtACR2-fRed in LC neurons (bottom): representative coronal images showing CAV2-PRS-stGtACR2-fRed expression (left column, red), labeling of DBH+ neurons (middle column, green), and their overlay (right column, yellow). (**B**) Whole-cell current-clamp recording from LC neurons in pontine slice ($n = 10$ rats, one to three neurons per rat) showing the spike discharge evoked by current injection is prevented by a brief pulse of light (473 nm, 200 ms x 4 mW) to activate the stGtACR2, a silencing effect seen across recordings from transduced LC neurons (data from response to 175-pA pulse; $P = 0.002$, Wilcoxon matched pairs; $n = 10$ neurons), whereas no effect of light was seen in nontransduced LC neurons in the same slices ($n = 7$ neurons). (**C**) Representative data from two recordings of neuronal clusters in the same CAV2-PRS-stGtACR2-fRed transduced rat. (Left) Action potential waveforms, (middle) raster plots and PSTH of inhibitory responses to different laser durations (in blue, 200, 1000, and 5000 ms), and (right) LC neuron with typical biphasic response to contralateral toe pinch, abolished by concurrent illumination. (**D**) Bar graph shows significant decrease in the firing rate of LC neurons upon 1 s of laser illumination ($n = 13$ units from two rats; nine trials, on average, per unit; ***$P < 0.001$, paired t test). (**E**) Representative pupil size traces (gray lines represent single trials, and black lines represent average of the trials) during 3 s (left) and 10 s (right) of laser illumination. (**F**) Bar graph shows significant pupil constriction when LC was silenced in a duration-dependent manner (stGtACR2 in blue, $n = 6$ rats; control mCherry in gray, $n = 5$ rats, 5 to 15 trials per laser duration condition), *$P < 0.05$, Wilcoxon test.

Fig. 6. Optogenetic LC silencing decreases the probability of SEAs. (A) Schematic of three conditions in LC opto-silencing arousal threshold experiments. Top: Presentation of sound (S) only (85-dB SPL); middle: same sound played simultaneously with laser stimulation (SL); bottom: same sound played 2 s after laser onset (SafterL). Laser duration was continuous for 5 s. **(B)** Probability of awakening as a function of the three conditions in rats expressing stGtACR2-fRed (blue, $n = 6$ rats) and mCherry control (gray, $n = 5$ rats) in NREM sleep (left) and REM sleep (right) (*$P < 0.05$ and **$P < 0.01$, paired t test). **(C)** Probability of awakenings from NREM sleep in each session per rat expressing stGtACR2-fRed. On average, per session and for each condition (S/SL/SafterL), 71 trials occurred during NREM sleep, and 20 trials occurred during REM sleep.

and 8.59 ± 2.10% decrease for SL and SafterL, respectively; $n = 6$) with a more pronounced decrease when baseline LC activity was silenced before sound onset (Fig. 6, B and C). Unlike the association between LC excitation and reduced spindles, LC silencing did not significantly affect spindle occurrence, although there was a trend toward increased spindle events ($P = 0.068$ via one-tailed paired t test; $n = 6$).

DISCUSSION

Behavioral unresponsiveness is a major characteristic of sleep that persists despite the danger it presents (predation). However, little is known about the neural mechanisms that mediate reduced responsiveness in the face of external sensory events and what underlies the variability in SEA probability between species and between individuals. Here, we show the role of LC-NE activity in mediating sensory-evoked arousal threshold during sleep. After validating

an experimental paradigm to quantify auditory arousal threshold in freely sleeping rats, we tested the link between LC-NE activity and SEAs. We established a relationship between baseline tonic LC activity and the probability of SEA and found that pharmacologically decreasing NE signaling reduced SEA probability. Minimal optogenetic LC excitation increased SEA probability during both NREM and REM sleep, while optogenetic silencing decreased SEA probability during NREM sleep, especially when silencing began shortly before sound onset. These results causally link activity in the LC to sensory stimulus–evoked awakening and support the idea that the absence of LC activity during sleep is responsible for the elevation of arousal thresholds.

Mechanisms controlling sensory-evoked awakening
Multiple overlapping neuromodulatory systems are implicated in sleep-wake regulation, including noradrenaline, histamine, acetylcholine,

hypocretin, and dopamine (5, 6). Strong activation of any of these systems promotes arousal, whereas their inhibition reduces wakefulness. Our results present several previously unknown findings. They go beyond neuromodulatory mechanisms controlling spontaneous awakening and highlight a key role for the LC-NE system in mediating sensory-evoked awakening in a natural context. Moreover, LC-NE activity modulates arousal threshold during sleep in a graded probabilistic manner. Given the overlap in neuromodulatory activities, other mechanisms likely also contribute to this process, as was shown for dorsal raphe dopamine activity (10). Wakefulness does not depend on one exclusive system, because even simultaneous lesions of histaminergic, noradrenergic, and cholinergic neurons do not robustly affect daily levels of wakefulness (30). Given that being able to wake up in response to external stimuli is crucial for survival, overlapping mechanisms likely contribute.

The mechanisms downstream from LC that modulate SEAs remain unclear. Our optogenetic experiments targeted LC cell bodies, and future studies are needed to determine the roles of NE (and dopamine) release at specific projection targets. While LC has been typically regarded as a relatively homogeneous nucleus, some recent studies challenge this view and suggest that LC subpopulations have distinct projections that serve different functions (31). Downstream effects of LC on SEAs could be mediated through direct cortical projections, where α-adrenergic receptors mediate cortical desynchronization (32). The LC may also act through thalamic projections. Infusion of NE (or LC stimulation) increases thalamic excitability, suppresses ongoing rhythmic activity (32), and accelerates emergence from anesthesia (33). Other possibilities are that LC affects regions that promote motor output or other modulatory centers such as the basal forebrain, where it activates cholinergic wake-promoting neurons and inhibits GABAergic sleep-promoting neurons. Infusion of β-or α1-receptor agonists into the basal forebrain causes SWA suppression and promotes awakening (34). LC projections to the hypothalamus, the amygdala, or other regions could also be involved.

A causal link between LC activity and pupil size

Pupil size is a marker of arousal and is often used to indirectly infer LC-NE activity levels across multiple species (35). Pupil size is tightly correlated with LC activity in monkeys (36, 37) and humans (38) and with cortical noradrenergic activity in mice (39, 40). In addition, electrical stimulation of LC causally affects pupil size (36, 41). Here, cell type–specific LC optogenetic establishes a robust causal bidirectional influence of LC activity on pupil size. Under light anesthesia, LC optogenetic activation drives large pupil dilation, while optogenetic silencing causes a modest but consistent pupil constriction, possibly reflecting a "floor" effect related to anesthesia. Our results in rats support a recently published study in mice (40) in showing that LC activity is sufficient to bidirectionally alter pupil dilation. LC-mediated pupil dilation may act through disinhibition of parasympathetic pathways (e.g., via cholinergic preganglionic neurons of the Edinger-Westphal nucleus controlling the sphincter muscle) with possible contribution of sympathetic pathways controlling the iris dilator muscle (41, 42). Our results provide a robust experimental framework to explore the precise mediating pathways in detail.

Tonic and phasic LC activity

The LC shows two types of activity: a tonic mode that is high in wakefulness and low in sleep implicated also in arousal, stress, anxiety, and pain processing, and a phasic mode that occurs during presen-

tation of salient stimuli, behavioral tasks, and reward anticipation (43). Our results highlight a role for tonic (but not phasic) LC activity in SEAs. For example, SEA probability was lower when LC silencing started before sound presentation than when LC silencing began simultaneously with the sound (Fig. 6B). In contrast, phasic sound-evoked LC responses were not linked to SEAs and were inversely proportional to levels of baseline tonic LC firing. The link between tonic LC activity and SEAs observed here, together with the link between tonic LC activity and anxiety (18), suggests how anxiety may promote awakenings (44). An active inference model recently proposed that LC activity represented a state-action prediction error where uncertainty was reflected in increased LC activity, which, in turn, promoted behavioral flexibility in behaving agents (45). This may be extended to sleep states where the observed tonic LC activity represents uncertainty about internal state and influences the probability of response (awakening) to a sensory stimulus (sound). Along this line, LC-NE activity may be an important factor driving variability in arousal threshold across individuals. We were surprised that phasic LC activity was not related to SEA probability, because it is reported to be related to salient stimuli. Thus, the mechanisms that underlie more frequent awakening in response to behaviorally relevant stimuli remain to be elucidated (3). While the current results indicate that LC activity robustly modulates SEA, it remains unclear to what extent this co-occurs with corresponding response modulations along sensory pathways. While LC-NE signaling modifies response fidelity across sensory modalities and species (43), it is unlikely that lower LC-NE activity simply "gates" propagation of auditory signals to the cortex, because auditory responses in primary cortex are largely comparable across vigilance states (46–48). Instead, tonic LC activity that drives SEAs may facilitate sensory processing downstream from primary regions by acting at higher-order regions or nonsensory pathways to promote awakenings.

In summary, we show that low LC activity during sleep plays a key role in mediating reduced responsiveness to sensory stimuli, thereby revealing a mechanism that controls how sleep is maintained in the face of external events.

MATERIALS AND METHODS
Animals

All experimental procedures at the University of Tel Aviv including animal handling, surgery, and experiments followed the National Institutes of Health *Guide for the Care and Use of Laboratory Animals* and were approved by the Institutional Animal Care and Use Committee. All experimental procedures at the University of Bristol conformed to the UK Animals (Scientific Procedures) Act 1986 and were approved by the University Animal Welfare and Ethical Review Board. Adult male Long-Evans rats (supplier, e.g., Rat Resource & Research Center, 8 to 12 weeks old at the time of surgery) were used for arousal threshold, pharmacological, and optogenetic experiments, except for acute opto-silencing where adult Lister Hooded rats were used (supplied by Charles River, 9 to 12 weeks old at time of surgery). Adult male Wistar rats (supplier Harlan Israel, 8 to 12 weeks old at the time of surgery) were used for chronic recordings. Rats were housed individually in transparent Plexiglas cages at constant temperature (20° to 23°C), humidity (40 to 70%), and circadian cycle (12-hour light/dark cycle, starting at 10:00 a.m.). Food and water were available ad libitum.

All behavioral and electrophysiological experiments were performed between 10:00 a.m. and 10:00 p.m. A few days before surgery, rats were placed in their home cage for habituation to the experimental environment.

Viral vectors

Viral vectors included CAV2-PRS-hChR2(H134R)-mCherry for LC opto-excitation (9) and CAV2-PRS-stGtACR2-fRed [for LC opto-silencing—based on (29)]. CAV2 vector titers were between 5×10^{12} and 14×10^{12} physical particles (pp)/ml, and 1×10^9 pp were typically injected to the LC. The generation and validation of CAV2-PRS-ChR2-mCherry for selective LC opto-excitation are described in our previous work (9). In brief, a 240–base pair PRSx8 synthetic promoter sequence was used that restricts the expression of the transgene to a subset of neurons that express the Phox2 transcription factor, which are predominantly catecholaminergic. For control animals, a double injection of CAV2-PRS-Cre-V5 (×10 dilution) and AAV5-EF1a-DIO-mCherry (Viral Core Facility, University of Zurich) was performed in a 1:1 ratio (fig. S4). mCherry$^+$ neurons (95.4 ± 2.9%) coexpressed TH, and 24.8 ± 8.0% of TH$^+$ neurons were mCherry$^+$. CAV2-PRS-stGtACR2-fRed was generated using methods described in (49). Details of the construction are available upon request: Briefly, CAV2-PRS-stGtACR2-fRed contains the PRS promoter driving stGtACR2 in sequence with fRed, a monomeric fluorescent protein, and a poly-adenylation signal (polyA) from SV40. This cassette replaces the E1 region in a E1/E3-deleted, replication-defective CAV vector. Similarly, CAV2-PRS-Cre-V5 was generated in the Pickering Lab and has the same promoter with Cre recombinase and a V5 tag in the expression cassette.

Surgery

Before all surgical procedures, rats were anesthetized [with either isoflurane 4% by volume for induction and 1.5% for maintenance or with ketamine (50 µg/kg; Vetalar; Pharmacia, Sweden) and medetomidine (300 mg/kg; Domitor; Pfizer, UK)] and placed in a stereotaxic frame. Surgery was performed under sterile conditions, following procedures described in (47, 50). Under microscopic control, a craniotomy was made using a high-speed surgical drill. When a probe/optrode was implanted, the dura was carefully opened. Then, electrodes or injection needles were advanced into the brainstem after penetrating the pia mater while carefully avoiding vasculature. Two-component silicone gel (Kwik-Sil; World Precision Instruments, FL, USA) was applied to seal the craniotomy and protect the brain surface. After gel polymerization, dental acrylic was gently placed around the electrodes or optic fibers, fixing them to the skull. EEG screws were placed over the frontal and parietal cortices. Ground and reference screw electrodes were placed above the posterior parietal lobe (ChR2 and associated experiments as well as chronic LC recordings) or above the cerebellum (otherwise). Neck muscle electrodes were implanted bilaterally, and bipolar referencing was used for EMG. A custom-made EEG/EMG connector was fixed on the skull with dental cement for sleep recordings.

For all experiments (except for acute silencing recordings), viral vectors were injected to the LC (using a UMP3 Microsyringe Injector and a Micro4 Controller pump, and 33-gauge NanoFil needles World Precision Instruments, USA) unilaterally (for activation) or bilaterally (for silencing) at the following coordinates: anteroposterior (AP), λ −3.7 mm; mediolateral (ML), ±1.18 mm; dorsoventral (DV), 6.2 to 6.6 mm with rostral angulation of 15°; and at a rate of 100 nl/min

for 12 min (three injections of 400 nl for a total volume of 1.2 µl). For light stimulation/inhibition, an optic fiber [200-µm diameter, 0.22 numerical aperture (NA)] was implanted (MFC_200/240-0.22_10 mm_MF1.25_FLT, Doric Lenses) above the LC. Unilateral and bilateral fiber implants were used for LC opto-excitation and opto-silencing, respectively, as was the case for virus injections, at these coordinates: AP, λ −3.7 mm; ML, +1.21 mm; DV, 5.4 mm with rostral angulation of 15°. In acute silencing experiments, viral vector was injected to the LC (using a Neurostar injector-drill robot on a Kopf stereotaxic frame) at the following coordinates: AP, λ −2.1 mm; ML, +1.2 mm; DV, 5.3 to 5.8 mm with rostral angulation of 10°.

Electrophysiology and LC recordings
Brain slice recordings

Male Wistar rats were used for slice electrophysiology using previously described methods (17, 50). CAV2-PRS-stGtACR2-fRed was injected (0.69×10^9 to 1.38×10^9 PP in total) under recovery anesthesia [ketamine (50 mg/kg; Vetalar; Pharmacia) and medetomidine (300 µg/kg; Domitor; Pfizer)] at postnatal day 21. After burr hole formation, a dorsoventral injection track for a vector-filled, pulled glass pipette (tip diameter, 20 to 30 µm) was started at 1 mm lateral and 1 mm posterior to lambda with 10° rostral angulation. Four injections of 250 nl of vector were made at depths from −4.6 to −5.5 mm unilaterally to the LC. Rats were terminally anesthetized with isoflurane (5%) 14 to 21 days later and decapitated, and the brain was quickly removed and immediately chilled in ice-cold cutting solution (similar to the recording solution, but NaCl was reduced to 85 mM and substituted with sucrose 58.4 mM). Transverse slices (300 to 350 µm thick) of the pons were cut from dorsal to ventral using a vibratome (Linearslicer Pro 7; DSK) in cold (4°C) cutting solution.

After cutting, slices were kept at room temperature in carbogenated recording solution [126 mM NaCl, 2.5 mM KCl, 26 mM NaHCO₃, 1.25 mM NaH₂PO₄, 2 mM MgCl₂, 2 mM CaCl₂, and 10 mM D-glucose saturated with 95% O₂/5% CO₂ (pH 7.3); osmolality, 290 mosmol/liter] for at least 1 hour to recover before recording. Pontine slices were transferred into the recording chamber of an upright fluorescence microscope (DMLFSA; Leica Microsystems), superfused with artificial cerebrospinal fluid at a rate of 4 to 8 ml/min heated to 35°C. Borosilicate glass patch pipettes (Harvard Apparatus GC120F-10, resistances of 3 to 6 megaohms) were filled with internal solution (130 mM K-gluconate, 10 mM KCl, 10 mM Na-Hepes, 4 mM MgATP 4, 0.2 mM EGTA, and 0.3 mM Na₂GTP). Cells were identified under gradient contrast illumination and examined for transduction by epifluorescence illumination. Blue light [473 nm, Doric light-emitting diode (LED), 4 mW] was pulsed onto slices from an optical fiber (400-µm diameter) placed above the LC. Whole-cell voltage and current-clamp recordings were obtained with a Multiclamp 700A amplifier (Axon Instruments). All membrane potentials were corrected for a junction potential of 13 mV. The reversal potential for chloride ions using this combination of internal and external solutions was calculated as −68.7 mV. Data were acquired using a Power1401 A-D converter (CED) and displayed and analyzed with Spike2 software (CED, Cambridge Electronic Design).

Chronic experiments

In all chronic experiments, epidural EEGs (filtered 0.1 to 100 Hz), muscle tone EMG (filtered 10 to 100 Hz), and infrared video (except for in optogenetic experiment) were continuously recorded using a TDT RZ2 electrophysiology system, PZ amplifier, and RV2 video capture system (for pharmacological experiments) from Tucker Davis

Technologies (TDT), USA. For chronic LC recordings, a 16-channel linear silicon probe (177 μM^2 contact surface area, 100 μM between adjacent contacts; NeuroNexus, USA) mounted on a micro-drive was implanted above the LC (AP, λ −3.7 mm; ML, +1.15 to 1.18 mm; DV, 5.8 to 7.2 mm). After recovery and auditory habituation, the chronic micro-drive electrode was lowered 50 to 200 μm daily under light isoflurane sedation until we succeeded in recording from neurons responding to toe pinch stimulation. In total, we recorded 16 clusters from three rats (rat 1: nine clusters; rat 2: two clusters; and rat 3: five clusters).

Acute recordings
For acute opto-excitation recording, 3 weeks after viral vector injection, an optrode was lowered progressively in the LC [same electrode specifications as in chronic experiment (see above), coupled with a 100-μm core diameter optic fiber mounted 100 μm above the top electrode contact; NeuroNexus, USA].

For acute opto-silencing recordings, rats were anesthetized with urethane at a dose of 1.5 mg/kg body weight and fixed in a stereotaxic frame. Isoflurane (at 1 to 2%) was also initially used as a supplement to urethane for the craniotomy surgery. Two craniotomies were made, each consisting of a "window" of side length between 0.5 and 1 mm centered on target coordinates from lambda AP −2.1 mm, ML, 1.2 mm and AP +1.4, ML 1.2 mm. A tapered fiber optic (OptogeniX, type Lambda-B) was inserted via the caudal window at a 10° rostral angulation to a depth of ~5.5 mm from the surface of the brain. A 32-channel silicon recording probe (NeuroNexus, A1x32-Poly2-10mm-50s-177) was then inserted using a Narishige hydraulic manipulator (MWS31) via the rostral craniotomy, at an angle of −20° to depths of up to 8 mm from the brain surface. The probe signal was digitized using a 32-channel headstage (RHD2132, INTAN); the resulting signal was acquired and displayed using the Open Ephys recording system (51). LC neurons were identified initially by their pattern of spontaneous discharge (0.2 to 5 Hz); large-amplitude long-duration action potentials; and their biphasic response to hindpaw pinch (17). Once the LC was identified, the field was then illuminated (445 nm, 15 mW at the tip, Omicron PhoxX laser), and the effect on spike discharge was examined. Post hoc histological examination confirmed the position of the recording probe in the LC.

Optogenetic laser parameters
Blue stimulation at 447 nm for optogenetic excitation and silencing was delivered via lasers (CNI, China) coupled to optic fibers whose timing and intensity were automatically controlled via RZ2 (TDT). Light intensity at optic fiber tips was measured with a power meter (ThorLabs PM100D) before optic fiber insertion. Before starting opto-activation arousal threshold experiments (Fig. 4), we confirmed effective LC opto-excitation in each animal by verifying that strong laser stimulation (10 s at 10 Hz, 90-ms pulse duration, 20 mW) evoked reliable EEG desynchronization and sleep-wake transitions (Fig. 3C), as shown in (8, 9). Only rats that woke up from sleep in response to strong laser stimulation were included in subsequent experiments with auditory stimulation. Next, we adjusted the laser stimulation parameters (total duration, 3 s; pulse duration, 10 to 30 ms), such that laser stimulation alone did not reliably affect awakening probability.

Auditory stimulation
All experiments were conducted in a double-wall sound-attenuating acoustic chamber (Industrial Acoustics Company, Winchester, UK).

All sounds were stereo signals programmed in MATLAB, where one channel (containing a 1-s 4-kHz tone pip) was routed to the mono speaker in the chamber and the other channel was routed to the electrophysiology acquisition system. The sounds were transduced into voltage signals by a high-sampling rate (192 kHz) sound card (LynxTWO, Lynx, USA), amplified (SA1, TDT), and played free field through a magnetic speaker (MF1, TDT) mounted 35 cm above the animal. For optogenetic experiments, where precise synchronization between auditory and laser stimulation was required, sounds were digitally loaded from a PC and routed to the mono speaker via a TDT RZ2 system (TDT, USA). Tone pips played during arousal threshold experiments were with intensities in the range of 50- to 98-dB SPL with intervals of 55 to 105 s with ±15-s jitter (the louder the sounds were, the higher the interval was between sounds). Sound intensity levels (dB SPL) were measured at cage floor height.

Systemic pharmacology
For systemic pharmacology experiments (Fig. 1, C and D, and fig. S1), either detomidine (1 mg/kg; α2 agonist to reduce NE levels), yohimbine (1 mg/kg; α2 antagonist to increase NE levels), or saline (0.9% NaCl; 1 ml/g) was injected intraperitoneally in pseudorandom order, while rats were lightly sedated with isoflurane. Recordings and acoustic stimulation started 15 to 20 min after the injection.

Combined arousal threshold and optogenetic experiments
In opto-activation experiment, we used three separate experimental paradigms (on different days) to evaluate the effects of laser stimulation with pulses applied at either 5 Hz, 10 Hz, or "burst mode," where 10 pulses were delivered at 20 Hz, repeated every second for 3 s. Sounds consisted of 1-s 4-kHz tone pips presented at either 67- or 80-dB SPL. Each experiment lasted ~12 hours and included three conditions (Fig. 4A): (i) a "sound-only" condition (S), where tone pips were presented alone; (ii) a "sound with laser" condition (SL), where tone pips were presented during the last second of laser stimulation; and (iii) a "laser-only" condition (L), where laser stimulation was delivered without sounds. We recorded from eight rats expressing ChR-mCherry and from seven rats expressing mCherry only (total of 66 sessions; each session ~12 hours long).

In opto-silencing experiment, each experiment included three conditions: (i) a "sound-only" condition (S), where tone pips were presented alone; (ii) a "sound after laser" condition ("SafterL"), where tone pips were presented 2 s after laser onset; and (iii) a "sound with laser" condition (SL), where tone pips were presented simultaneously with the laser onset. Laser was applied for 5 s continuously. Each condition (S, SL, and SafterL) was compared to the other condition of the same-day session. We recorded from six rats expressing stGtACR2-fRed and five rats expressing mCherry only (total of 37 sessions; each session ~12 hours long).

Pupillometry
Rats were anesthetized with 1.5% isoflurane and placed in a stereotaxic frame. An optic fiber connected the implanted optic fiber ferrule to the 473-nm laser. The eye was illuminated with an infrared light and monitored continuously with a vision color camera (VGAC; TDT) synchronized to a dedicated RV2 video processor (TDT), allowing frame-by-frame synchronization between video data (30 frames/s) and laser stimulation. We examined the effects of different pulse durations (10 to 90 ms) on pupil size. For LC activation (Fig. 3, J to L), we applied unilateral laser stimulation to the LC while recording

from the contralateral pupil. For LC silencing (Fig. 5, E and F), we applied bilateral laser stimulation while recording from the left eye followed by the right eye, and then averaged the pupil size change of the two eyes. In control experiments, we applied unilateral (control for opto-excitation) or bilateral (control for opto-silencing) laser stimulation to the LC.

Histology
Tissue collection and fixation
Following all experiments (except acute silencing experiments), rats were perfused intracardially with saline (0.9% NaCl; 1 ml/g) followed by 4% paraformaldehyde (Merck) under deep isoflurane anesthesia. Brains were then extracted and fixed for 24 to 48 hours in 4% para-formaldehyde. Coronal brain sections were cut using Leica VT1000 S vibrating blade microtome at 50 μm. Then, sections were either kept free floating in phosphate-buffered saline (PBS) for immuno-histochemistry or mounted on glass slides and examined under bright-field microscopy. Following acute silencing experiments, rats were killed with an overdose of pentobarbital (Euthatal; 20 mg/100 g via intraperitoneal injection) and perfused transcardially with 0.9% NaCl followed by 4% formaldehyde in 0.1 M phosphate buffer (PB). Brains were removed and postfixed overnight before cryoprotection in 30% sucrose in 0.1 M PB. Sagittal tissue sections were then cut at 40-μm intervals using a freezing microtome.

Immunohistochemistry
The viral vector expression efficacy and specificity were evaluated histologically by double staining of free-floating sections. To this end, following all experiments (except acute silencing experiments), sections were washed three times in PBS (Hylabs) and then perme-abilized in PBST (PBS containing 0.1% Triton X-100; Merck). Next, sections were blocked in PBST containing 20% NGS (normal goat serum; Vector Laboratories) for 1 hour at room temperature and incubated with primary antibodies in PBST (containing 2% NGS) at 4°C for 24 to 36 hours. Primary antibodies were either against TH (chicken anti-TH, 1:500; ab76442, Abcam) and mCherry (mouse anti-mCherry, 1:500; ab125096, Abcam) for activation or against dopamine beta hydroxylase (mouse anti-DBH, 1:500; MAB308, Merck Millipore) and fRed (rabbit anti-tRFP, 1:500; AB233, Evrogen) for silencing. After three washes in PBS, sections were incubated with secondary antibodies conjugated to fluorophores [either Alexa Fluor 488 goat anti-chicken (1:1000; ab150173, Abcam) and Alexa Fluor 594 goat anti-mouse(1:1000; ab150120, Abcam) for activation, or Alexa Fluor 488 goat anti-mouse (1:1000; ab150117, Abcam) and Alexa Fluor 594 goat anti-rabbit (1:1000; ab150080, Abcam) for silencing] in PBST containing 2% NGS for 1.5 hours at room tem-perature. After three washes in PBS and once in PBST, sections were mounted onto glass slides and coverslipped with aqueous mounting medium (Thermo Scientific, catalog no. 9990412). Following acute silencing experiments, sections were mounted on slides and perme-abilized in 0.1 M PB containing 0.3% Triton X-100 (Sigma) and then blocked for 45 min in 0.1 M PB containing 0.3% Triton X-100 (Sigma) and 5% NGS (Sigma). Sections were then incubated on-slide with primary antibodies against DBH [mouse anti-DBH, 1:2000; MAB308, Millipore (Chemicon)] and fRed (rabbit anti-tRFP, 1:500; AB233, Evrogen) in PB containing 5% goat serum and 0.3% Triton X-100 for 16 hours. After removal of primary antibodies, tissue sections were washed twice in PB and then incubated with appropriate secondary antibodies conjugated to fluorophores (Alexa Fluor 488 goat anti-mouse and Alexa Fluor 594 goat anti-rabbit, both at 1:1000 dilution)

in PB containing 0.3% Triton X-100 and 5% NGS at room temperature for 4 hours. Sections were again washed twice in PB and coverslipped with FluorSave mounting medium.

Fluorescence microscopy
Images were acquired by a Leica STED high-resolution laser scan-ning confocal microscope (Leica, Wetzlar, Germany) and a 20 oil/1.4 NA objective. Quantification of extent of colocalization was carried out by Imaris software (Bitplane, Zurich, Switzerland).

For histology of rats used in acute silencing experiments, images were acquired by Zeiss Axisoskop2 with pE2 LED excitation system (CoolLED, UK) and analyzed using a Zeiss Axiocam and AxioVision software. For tissue from acute optogenetic silencing experiments, images were acquired using a Leica DMI6000 inverted epifluorescence microscope equipped with Leica DFC365FX monochrome digital camera and Leica LAS-X acquisition software.

Data analysis
Sleep staging and awakenings
Wakefulness was defined by low-amplitude, high-frequency EEG activity, co-occurring with high tonic EMG activity with occasional phasic EMG bursts. In chronic LC recording experiments, we divided the wake-fulness epochs between active wake (grooming, eating, and exploration) and quiet wake based on video recording. NREM sleep was defined by high-amplitude, low-frequency EEG, co-occurring with reduced EMG tone. REM sleep was defined by low-amplitude, high-frequency EEG dominated by posterior theta activity co-occurring with flat EMG, as in (47).

In arousal threshold experiments, each experimental trial was visually inspected, and those occurring during sleep were categorized as either eliciting behavioral awakening or maintained sleep. Behavioral awakening was declared if wake-like EEG flattening (without dominant theta) was present within 3 s from sound onset and lasted for at least 3 s. A substantial percentage of such intervals was accompanied by EMG changes (fig. S3), but these did not constitute a necessary condition because changes in neck EMG were not always present, even in cases where video showed clear awakening. When laser was presented alone, behavioral awakening was declared if the changes described above occurred in the same 3 s. Arousals could be followed by a wake period or by return to sleep (Fig. 1A). All other trials were categorized as maintained sleep.

Arousal threshold analysis
We compared awakening probability across sound intensities for NREM sleep and REM sleep separately (Fig. 1B), between drugs for the three sound intensities and sleep stages separately (Fig. 1D), and as a function of time elapsed after drug injection (fig. S1A).

In combined arousal threshold and optogenetic experiments, awakening probability was computed separately for NREM sleep and REM sleep, across conditions (S/SL/L), and across sound intensities (67/80-dB SPL). Specific conditions with less than 15 trials per con-dition (e.g., 67-dB SPL in REM sleep) were excluded from analysis.

To assess true synergism between NE activity and sounds above and beyond their expected independent effects, we calculated the expected cumulative effect of the sound alone and the laser alone as follows: %S + (100 − %S) × (%L)/100 (where %S is the awakening percentage for sound only, and %L is the awakening percentage for laser alone; see horizontal lines in Fig. 4B). We then compared it to the observed awakening probability in the SL condition via two-way repeated-measures (RM) ANOVA [between conditions (S/SL) and laser param-eters (5 Hz/10 Hz/burst) in NREM and REM sleep followed by paired t test corrected with false discovery rate; Fig. 4 and fig. S2].

EEG and EMG analyses

To calculate the time-varying amplitude of the EEG in specific frequency bands (0.5 to 4 Hz for delta and 5 to 9 Hz for theta), a notch filter was first applied around 50 Hz, and then the instantaneous amplitude was obtained by taking the absolute value of the Hilbert transform of the band-passed signal. Amplitude signals were then smoothed by a moving average filter (with 0.5-s window) and normalized using z score relative to the baseline (2 s before sound). We then averaged the amplitude after the sound (0 to 6 s) and compared between trials followed by awakenings and trials followed by maintained sleep. We analyzed the EMG signal by first normalizing using z score and calculated the increase in the root mean square (RMS) after the sound (0 to 6 s) compared with the RMS of the baseline EMG activity (2 s before sound) in trials followed by awakenings versus trials followed by maintained sleep. We calculated the fast Fourier transform (FFT) of baseline EEG activity for each trial and found decrease in delta power (0.5 to 4 Hz) in trials followed by awakenings compared with trials followed by maintained sleep. These comparisons were done via one-tailed paired t test for $n = 9$ rats (three from ChR2-mCherry, three from mCherry, and three from stGtACR2-fRed). We also calculated the FFT of baseline EEG activity for the silencing chronic experiment and found increase in delta power (0.5 to 4 Hz) in trials with laser compared with trials without laser. These comparisons were done via one-tailed paired t test for $n = 17$ sessions (six rats injected with stGtACR2-fRed).

Sleep spindles

Individual spindles were detected automatically in the EEG as in (23). Briefly, we identified events >2 SD over the mean of the 10- to 16-Hz band-pass–filtered signal and verified that increased power was specific to this range and not broadband. We then counted the number of spindle peaks that occurred in the 1.5 s before sound onset and compared laser on trials to laser off trials via paired t test.

Locomotor activity analysis

Rat position and movement were analyzed with a custom video software written in MATLAB that determines the animal's center of mass and movement based on subtraction of consecutive images. After initial input from the user [who marks the initial animal location via a dedicated graphical user interface (GUI)], the software subtracts consecutive frames and, based on the number of pixels that were changed, estimates the degree of movement. Position and movements were compared between saline and yohimbine experiments via paired t tests (fig. S1D). We then calculated and compared the increase in locomotion time and distance traveled.

Pupillometry

To extract pupil area, video images were first cropped around the eye. A mask based on the median values was applied, and the best centrally fitted circle was selected using the "regionprops" function in MATLAB. For each trial separately, pupil area was normalized by the average baseline pupil area in the 1 s preceding trial onset, and percent change dynamics were calculated for the [−5 25]s interval around laser stimulation. Trials were then averaged for each animal and condition separately (~15 trials per condition) to generate time courses as seen in Fig. 3K. Statistically significant changes in pupil area in relation to baseline and between-parameters conditions (e.g., 70-ms versus 90-ms pulse duration) were evaluated via Wilcoxon signed-ranked test. The peak (trough) in pupil size was found by searching for the maximal (or minimal) value in the pupil size vector (excitation or silencing experiments, respectively) between 1 s before laser offset and 4 s after laser offset.

Unit identification and spike sorting

Neuronal clusters were identified using the "wave_clus" software package (52) as described previously. For acute activation recordings, extracellular recordings were high-pass filtered above 300 Hz, and then a threshold at 5 SD above the median noise level was computed (for chronic recordings, a similar threshold was set manually). Then, detected events were clustered using superparamagnetic clustering and were categorized as noise or neuronal clusters. For acute inhibition recordings, units were identified using the KiloSort clustering package (53). The Python-based clustering package Phy (https://github.com/kwikteam/phy-contrib) was then used to manually curate Kilosort output to select only well-isolated single units with clear refractory periods and to remove artifacts.

Analysis of spiking activity

For analysis of spontaneous (Fig. 2B) and sound-evoked (Fig. 2C) LC activity, data were first divided into vigilance states (active quiet, quiet wake, NREM sleep, NREM-REM sleep transitions, and REM sleep) according to EEG, EMG, and video (see above). Baseline tonic activity was calculated by averaging the firing rate 2 s before sound onset for each cluster and compared between states and within NREM sleep depending on whether the sound led to an awakening or not (Fig. 2, D and E). Percentage increase in awakening was calculated as follows: $\%\text{Increase} = \frac{\text{FR (awakenings} - \text{maintained sleep)}}{\text{FR [max(awakening, maintened sleep)]}} \times 100$. Sound-evoked firing was calculated by averaging the firing rate during the 100 ms after sound onset for each cluster and compared between states (Fig. 2C). All comparisons were done via a paired t test.

REFERENCES AND NOTES

1. R. C. Anafi, M. S. Kayser, D. M. Raizen, Exploring phylogeny to find the function of sleep. *Nat. Rev. Neurosci.* **20**, 109–116 (2019).
2. D. Neckelmann, R. Ursin, Sleep stages and EEG power spectrum in relation to acoustical stimulus arousal threshold in the rat. *Sleep* **16**, 467–477 (1993).
3. I. Oswald, A. M. Taylor, M. Treisman, Discriminative responses to stimulation during human sleep. *Brain* **83**, 440–453 (1960).
4. K. A. Busby, L. Mercier, R. T. Pivik, Ontogenetic variation in auditory arousal threshold during sleep. *Psychophysiology* **31**, 182–188 (1994).
5. S.-H. Lee, Y. Dan, Neuromodulation of brain states. *Neuron* **76**, 209–222 (2012).
6. M. L. Lőrincz, A. R. Adamantidis, Monoaminergic control of brain states and sensory processing: Existing knowledge and recent insights obtained with optogenetics. *Prog. Neurobiol.* **151**, 237–253 (2017).
7. A. R. Adamantidis, F. Zhang, A. M. Aravanis, K. Deisseroth, L. de Lecea, Neural substrates of awakening probed with optogenetic control of hypocretin neurons. *Nature* **450**, 420–424 (2007).
8. M. E. Carter, O. Yizhar, S. Chikahisa, H. Nguyen, A. Adamantidis, S. Nishino, K. Deisseroth, L. de Lecea, Tuning arousal with optogenetic modulation of locus coeruleus neurons. *Nat. Neurosci.* **13**, 1526–1533 (2010).
9. Y. Li, L. Hickey, R. Perrins, E. Werlen, A. A. Patel, S. Hirschberg, M. W. Jones, S. Salinas, E. J. Kremer, A. E. Pickering, Retrograde optogenetic characterization of the pontospinal module of the locus coeruleus with a canine adenoviral vector. *Brain Res.* **1641**, 274–290 (2016).
10. J. R. Cho, J. B. Treweek, J. E. Robinson, C. Xiao, L. R. Bremner, A. Greenbaum, V. Gradinaru, Dorsal raphe dopamine neurons modulate arousal and promote wakefulness by salient stimuli. *Neuron* **94**, 1205–1219.e8 (2017).
11. C. G. Herrera, M. C. Cadavieco, S. Jego, A. Ponomarenko, T. Korotkova, A. Adamantidis, Hypothalamic feedforward inhibition of thalamocortical network controls arousal and consciousness. *Nat. Neurosci.* **19**, 290–298 (2016).
12. A. Eban-Rothschild, G. Rothschild, W. J. Giardino, J. R. Jones, L. de Lecea, VTA dopaminergic neurons regulate ethologically relevant sleep-wake behaviors. *Nat. Neurosci.* **19**, 1356–1366 (2016).
13. G. Aston-Jones, F. E. Bloom, Activity of norepinephrine-containing locus coeruleus neurons in behaving rats anticipates fluctuations in the sleep-waking cycle. *J. Neurosci.* **1**, 876–886 (1981).

14. C. W. Berridge, M. E. Page, R. J. Valentino, S. L. Foote, Effects of locus coeruleus inactivation on electroencephalographic activity in neocortex and hippocampus. *Neuroscience* **55**, 381–393 (1993).

15. M. E. Carter, J. Brill, P. Bonnavion, J. R. Huguenard, R. Huerta, L. de Lecea, Mechanism for hypocretin-mediated sleep-to-wake transitions. *Proc. Natl. Acad. Sci. U.S.A.* **109**, E2635–E2644 (2012).

16. S. J. Sara, S. Bouret, Orienting and reorienting: The Locus coeruleus mediates cognition through arousal. *Neuron* **76**, 130–141 (2012).

17. L. Hickey, Y. Li, S. J. Fyson, T. C. Watson, R. Perrins, J. Hewinson, A. G. Teschemacher, H. Furue, B. M. Lumb, A. E. Pickering, Optoactivation of locus ceruleus neurons evokes bidirectional changes in thermal nociception in rats. *J. Neurosci.* **34**, 4148–4160 (2014).

18. J. G. McCall, R. Al-Hasani, E. R. Siuda, D. Y. Hong, A. J. Norris, C. P. Ford, M. R. Bruchas, CRH engagement of the locus coeruleus noradrenergic system mediates stress-induced anxiety. *Neuron* **87**, 605–620 (2015).

19. L. C. Manella, N. Petersen, C. Linster, Stimulation of the locus coeruleus modulates signal-to-noise ratio in the olfactory bulb. *J. Neurosci.* **37**, 11605–11615 (2017).

20. M. S. Hunsley, R. D. Palmiter, Altered sleep latency and arousal regulation in mice lacking norepinephrine. *Pharmacol. Biochem. Behav.* **78**, 765–773 (2004).

21. C. W. Berridge, R. A. España, Synergistic sedative effects of noradrenergic α_1- and β-receptor blockade on forebrain electroencephalographic and behavioral indices. *Neuroscience* **99**, 495–505 (2000).

22. J. A. Giovannitti Jr., S. M. Thoms, J. J. Crawford, Alpha-2 adrenergic receptor agonists: A review of current clinical applications. *Anesth. Prog.* **62**, 31–38 (2015).

23. Y. Sela, V. V. Vyazovskiy, C. Cirelli, G. Tononi, Y. Nir, Responses in rat core auditory cortex are preserved during sleep spindle oscillations. *Sleep* **39**, 1069–1082 (2016).

24. K. M. Swift, B. A. Gross, M. A. Frazer, D. S. Bauer, K. J. D. Clark, E. M. Vazey, G. Aston-jones, Y. Li, A. E. Pickering, S. J. Sara, G. R. Poe, Abnormal locus coeruleus sleep activity alters sleep signatures of memory consolidation and impairs place cell stability and spatial memory. *Curr. Biol.* **28**, 3599–3609.e4 (2018).

25. N. K. Totah, R. M. Neves, S. Panzeri, N. K. Logothetis, O. Eschenko, The locus coeruleus is a complex and differentiated neuromodulatory system. *Neuron* **99**, 1055–1068.e6 (2018).

26. J. M. Cedarbaum, G. K. Aghajanian, Activation of locus coeruleus neurons by peripheral stimuli: Modulation by a collateral inhibitory mechanism. *Life Sci.* **23**, 1383–1392 (1978).

27. R. D. Wimmer, S. Astori, C. T. Bond, Z. Rovó, J. Y. Chatton, J. P. Adelman, P. Franken, A. Lüthi, Sustaining sleep spindles through enhanced SK2-channel activity consolidates sleep and elevates arousal threshold. *J. Neurosci.* **32**, 13917–13928 (2012).

28. T. T. Dang-Vu, S. M. McKinney, O. M. Buxton, J. M. Solet, J. M. Ellenbogen, Spontaneous brain rhythms predict sleep stability in the face of noise. *Curr. Biol.* **20**, R626–R627 (2010).

29. M. Mahn, L. Gibor, P. Patil, K. Cohen-Kashi Malina, S. Oring, Y. Printz, R. Levy, I. Lampl, O. Yizhar, High-efficiency optogenetic silencing with soma-targeted anion-conducting channelrhodopsins. *Nat. Commun.* **9**, 4125 (2018).

30. C. Blanco-Centurion, D. Gerashchenko, P. J. Shiromani, Effects of saporin-Induced Lesions of three arousal populations on daily levels of sleep and wake. *J. Neurosci.* **27**, 14041–14048 (2007).

31. D. J. Chandler, P. Jensen, J. G. McCall, A. E. Pickering, L. A. Schwarz, N. K. Totah, Redefining noradrenergic neuromodulation of behavior: Impacts of a modular locus coeruleus architecture. *J. Neurosci.* **39**, 8239–8249 (2019).

32. D. A. McCormick, Neurotransmitter actions in the thalamus and cerebral cortex and their role in neuromodulation of thalamocortical activity. *Prog. Neurobiol.* **39**, 337–388 (1992).

33. E. M. Vazey, G. Aston-Jones, Designer receptor manipulations reveal a role of the locus coeruleus noradrenergic system in isoflurane general anesthesia. *Proc. Natl. Acad. Sci. U.S.A.* **111**, 3859–3864 (2014).

34. C. W. Berridge, Noradrenergic modulation of arousal. *Brain Res. Rev.* **58**, 1–17 (2007).

35. M. J. Mcginley, M. Vinck, J. Reimer, R. Batista-brito, E. Zagha, C. R. Cadwell, A. S. Tolias, J. A. Cardin, D. A. McCormick, Waking state : Rapid variations modulate neural and behavioral responses. *Neuron* **87**, 1143–1161 (2015).

36. S. Joshi, Y. Li, R. M. Kalwani, J. I. Gold, Relationships between pupil diameter and neuronal activity in the locus coeruleus , colliculi , and cingulate cortex. *Neuron* **89**, 221–234 (2016).

37. C. Varazzani, A. San-Galli, S. Gilardeau, S. Bouret, Noradrenaline and dopamine neurons in the reward/effort trade-off: A direct electrophysiological comparison in behaving monkeys. *J. Neurosci.* **35**, 7866–7877 (2015).

38. P. R. Murphy, R. G. O'Connell, M. O'Sullivan, I. H. Robertson, J. H. Balsters, Pupil diameter covaries with BOLD activity in human locus coeruleus. *Hum. Brain Mapp.* **35**, 4140–4154 (2014).

39. J. Reimer, M. J. McGinley, Y. Liu, C. Rodenkirch, Q. Wang, D. A. McCormick, A. S. Tolias, Pupil fluctuations track rapid changes in adrenergic and cholinergic activity in cortex. *Nat. Commun.* **7**, 13289 (2016).

40. V. Breton-Provencher, M. Sur, Active control of arousal by a locus coeruleus GABAergic circuit. *Nat. Neurosci.* **22**, 218–228 (2019).

41. Y. Liu, C. Rodenkirch, N. Moskowitz, B. Schriver, Q. Wang, Dynamic lateralization of pupil dilation evoked by locus coeruleus activation results from sympathetic, not parasympathetic, contributions. *Cell Rep.* **20**, 3099–3112 (2017).

42. O. Lowenstein, I. E. Loewenfeld, The sleep-waking cycle and pupillary activity. *Ann. N. Y. Acad. Sci.* **117**, 142–156 (1964).

43. B. D. Waterhouse, R. L. Navarra, The locus coeruleus-norepinephrine system and sensory signal processing: A historical review and current perspectives. *Brain Res.* **1709**, 1–15 (2019).

44. L. D. Sanford, D. Suchecki, P. Meerlo, Stress, arousal, and sleep. *Curr. Top. Behav. Neurosci.* **25**, 379–410 (2014).

45. A. C. Sales, K. J. Friston, M. W. Jones, A. E. Pickering, R. J. Moran, Locus coeruleus tracking of prediction errors optimises cognitive flexibility: An active inference model. *PLOS Comput. Biol.* **15**, e1006267 (2019).

46. E. B. Issa, X. Wang, Sensory responses during sleep in primate primary and secondary auditory cortex. *J. Neurosci.* **28**, 14467–14480 (2008).

47. Y. Nir, V. V. Vyazovskiy, C. Cirelli, M. I. Banks, G. Tononi, Auditory responses and stimulus-specific adaptation in rat auditory cortex are preserved across NREM and REM sleep. *Cereb. Cortex* **25**, 1362–1378 (2013).

48. A. J. Krom, A. Marmelshtein, H. Gelbard-Sagiv, A. Tankus, D. Hayat, I. Matot, I. Strauss, F. Fahoum, M. Soehle, J. Boström, F. Mormann, I. Fried, Y. Nir, Anesthesia-induced loss of consciousness disrupts auditory responses beyond primary cortex. *bioRxiv*, 502385 (2018).

49. D. del Rio, B. Beucher, M. Lavigne, A. Wehbi, I. Gonzalez Dopeso-Reyes, I. Saggio, E. J. Kremer, CAV-2 vector development and gene transfer in the central and peripheral nervous systems. *Front. Mol. Neurosci.* **12**, 71 (2019).

50. S. Hirschberg, Y. Li, A. Randall, E. J. Kremer, A. E. Pickering, Functional dichotomy in spinal- vs prefrontal-projecting locus coeruleus modules splits descending noradrenergic analgesia from ascending aversion and anxiety in rats. *eLife* **6**, e29808 (2017).

51. J. H. Siegle, A. C. López, Y. A. Patel, K. Abramov, S. Ohayon, J. Voigts, Open EPHYS: An open-source, plugin-based platform for multichannel electrophysiology. *J. Neural Eng.* **14**, 045003 (2017).

52. R. Q. Quiroga, Z. Nadasdy, Y. Ben-Shaul, Unsupervised spike detection and sorting with wavelets and superparamagnetic clustering. *Neural Comput.* **16**, 1661–1687 (2004).

53. M. Pachitariu, N. Steinmetz, S. Kadir, M. Carandini, K. D. Harris, Kilosort: Realtime spike-sorting for extracellular electrophysiology with hundreds of channels. *bioRxiv*, 1–14 (2016).